Chapter 4

Non-enzymatic electrochemical detection of glucose using nanoscale CuO/PEDOT-MoS_2 electrode

---

In last two chapters, the fabrication of electrochemical immunosensors is discussed highlighting material synthesis, process parameters and experimental steps that can be adjusted for better performance of the sensor. The major challenge with utilizing such enzymatic sensor is the proper storage of the fabricated immunosensor probes as biomolecules are vulnerable to temperature, pH and humidity. This leads to the essence of enzyme free electrochemical detection mechanisms. In this chapter, we have developed a non-enzymatic sensing protocol for efficient detection of glucose. Also, the influence of conducting polymer and 2D layered nanostructure on the electrochemical parameters of the electrode systems have also been examined.

4.1. Introduction

Monitoring of glucose level in human body has become an essential and most common diagnosis in medical emergencies as well as in most of the routine check-ups. Dealing with enzymatic sensors require some extra measures for storage, processing and handling of biomolecule-based immunosensor. So, people look for alternative yet attractive strategy like deploying non-enzymatic glucose sensors due to their lower cost, easy processing and storage, faster response, and long lifespan. As mentioned in section 1.1.3 of Chapter 1, some transition metals *e.g.*, cobalt, nickel, palladium, vanadium, copper, molybdenum, etc can exhibit glucose oxidizing activity in their oxide forms. Among them copper oxide (CuO) owns easy synthesis procedure, high abundancy, less toxicity, high catalytic activity, and long-time stability. This makes CuO a potential candidate for designing high performance enzyme free glucose sensor [181]. Besides, inclusion of conducting polymer and 2D layered nano structures as base substrate would not only increase the surface area of the electrodes for better incorporation of CuO but also synergically upgrade the conductivity and charge transfer kinetics of the nano composite [182-185].

In the present work, we have designed an efficient non-enzymatic sensing protocol for glucose by electrodepositing CuO nanoparticles (NPs) over PEDOT-MoS_2 composite matrix. The advantages of utilizing PEDOT-MoS_2 based composite system has been previously discussed in section 3.1 of Chapter 3. It is expected that deployment of CuO/PEDOT-MoS_2 based non-enzymatic glucose sensor would certainly find huge scope in fast, convenient, and smart sensing. A scheme which depicts the distribution of CuO NPs over the MoS_2 infiltrated PEDOT host polymer is shown in Figure 4.1. Also, the glucose oxidation by the electrocatalytic process of copper (Cu) reduction ($Cu^{III} \rightarrow Cu^{II}$) is clearly depicted in the same figure.

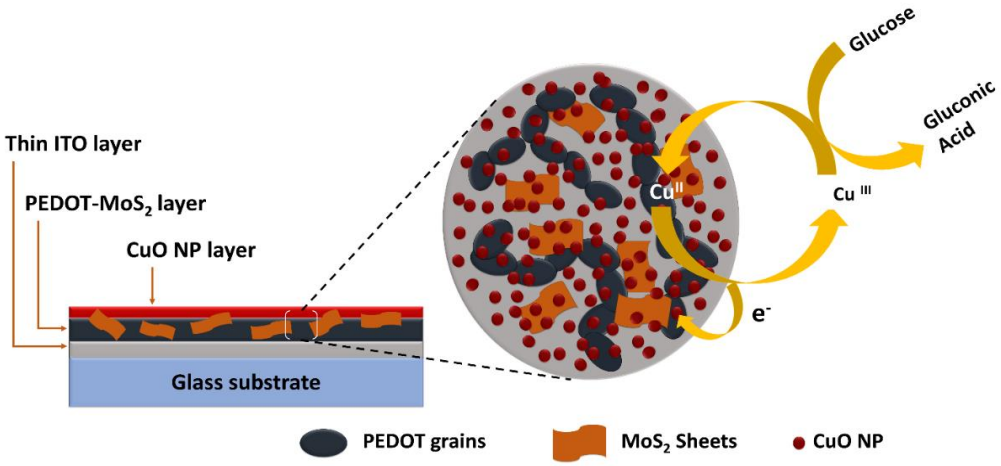

Figure 4.1: Schematic diagram of the glucose oxidation mechanism by as synthesized CuO/PEDOT-MoS_2/ITO electrode

4.2. Experimental

4.2.1 Electrodeposition of CuO nanoparticles

Electrodeposition of Cu nanoparticles over the ITO electrode was accomplished by chronoamperometry technique performed for 35 s in 0.1 M aqueous $CuSO_4$ solution at a fixed bias reduction potential of -0.9 V applied w.r.t. the Ag/AgCl reference electrode. The appearance of brown film over the ITO surface confirms the successful deposition of the Cu NPs. Later on, Cu NPs deposited electrode was treated with 0.1M NaOH solution for conversion of Cu NPs to CuO NPs.

4.2.2. Electrochemical synthesis of CuO/PEDOT/ITO

For the synthesis of CuO deposited PEDOT system, at first PEDOT film was electrodeposited over the ITO substrate by following the same method outlined in section 3.2.1 of Chapter 3. Afterwards, the film was allowed to dry in ambient environment

followed by deposition of CuO NPs over the PEDOT/ITO electrode (see section 4.2.1) to obtain CuO/PEDOT/ITO system.

4.2.3. Liquid exfoliation of MoS_2 nanosheets

In bulk form, these MoS_2 layers are held together by the weak van der Waal's force. So, MoS_2 can be exfoliated in the form of 2D nanosheets by using external energy through mechanical wave. Firstly, 90 mL of 1 mg/mL MoS_2 solution is prepared in a mixture of N-Methyl-2-pyrrolidone (NMP) and deionized water (1:1) sol in 3 different centrifuge tubes. They were subjected to sonication in a bath sonicator, for nearly 8 h. Following centrifugation (~2000 rpm) for 10 min, the decant (top $3/4^{th}$ part of the dispersed solution) was collected for each sample. The remaining sol was recentrifuged at ~ 3000 rpm, for 10 min and then, top half part of the supernatant was collected by pipette that contains the exfoliated MoS_2 sheets eventually [186].

4.2.4. Electrochemical synthesis of CuO/PEDOT-MoS_2/ITO

To fabricate CuO/PEDOT-MoS_2/ITO electrode, initially PEDOT-MoS_2 film was electrodeposited over ITO substrate. For this, we have considered an electrolyte solution having the same composition as depicted in section 3.2.1. Then 150 µL/mL of aqueous exfoliated MoS_2 dispersion (having MoS_2 concentration of 0.02 mg/mL) was added in the above solution and subjected to ultrasonication for 20 min that resulted uniform mixing. Then, electrodeposition of PEDOT-MoS_2 was executed via chronoamperometric method applying a dc bias voltage of +1.0 V w.r.t. Ag/AgCl for 70 s. Later on, CuO was electrodeposited over the PEDOT-MoS_2 yielding CuO/PEDOT-MoS_2 film coated over ITO surface.

4.3 Results and discussion

4.3.1. X-ray diffraction (XRD) and infra-red spectroscopy studies

The XRD patterns of CuO, PEDOT, CuO/PEDOT, PEDOT-MoS_2 and CuO/PEDOT-MoS_2 have been acquired over the diffraction angle, 2θ=10°-80° and shown collectively, in Figure 4.2(a). The sample preparation process for structural study is same as depicted in section 2.3.1. In the diffractogram of CuO deposited electrode; CuO (002) and Cu (111) peaks can be found at, 2θ= 36.5° and 43.3°; respectively (ICDD ref No. 00-041-0254) [187]. The sharp Cu (111) characteristic peak indicates high crystallinity of the electrodeposited CuO. However, no clear indication of the diffraction peaks can be ascertained for the PEDOT, shown in Figure 4.2(a)(ii), which is consistent with the earlier work. The appearance of other significant peaks at ~30.7°, 35.6°, 50.7° and 60.4° is ascribed to the ITO substrate

over which the PEDOT matrix is electrodeposited. The XRD pattern of CuO/PEDOT in curve-(iii) depicts a similar response like PEDOT in addition to Cu (111) peak located at $2\theta = 43.3^{o}$. Moreover, the characteristic diffraction peaks at $2\theta \sim 13.6^{o}$ and 14.7^{o} suggest the adequate incorporation of exfoliated MoS_2 in the PEDOT matrix [188]. Finally, in case of composite electrode system of CuO/PEDOT-MoS_2, the peaks of exfoliated MoS_2 get suppressed and the Cu (111) characteristic peak showed a slight shifting towards a lower diffraction angle (Figure 4.2(a)(v)). This is because, there is a change in lattice parameter due to the incorporation of CuO NPs over the composite system.

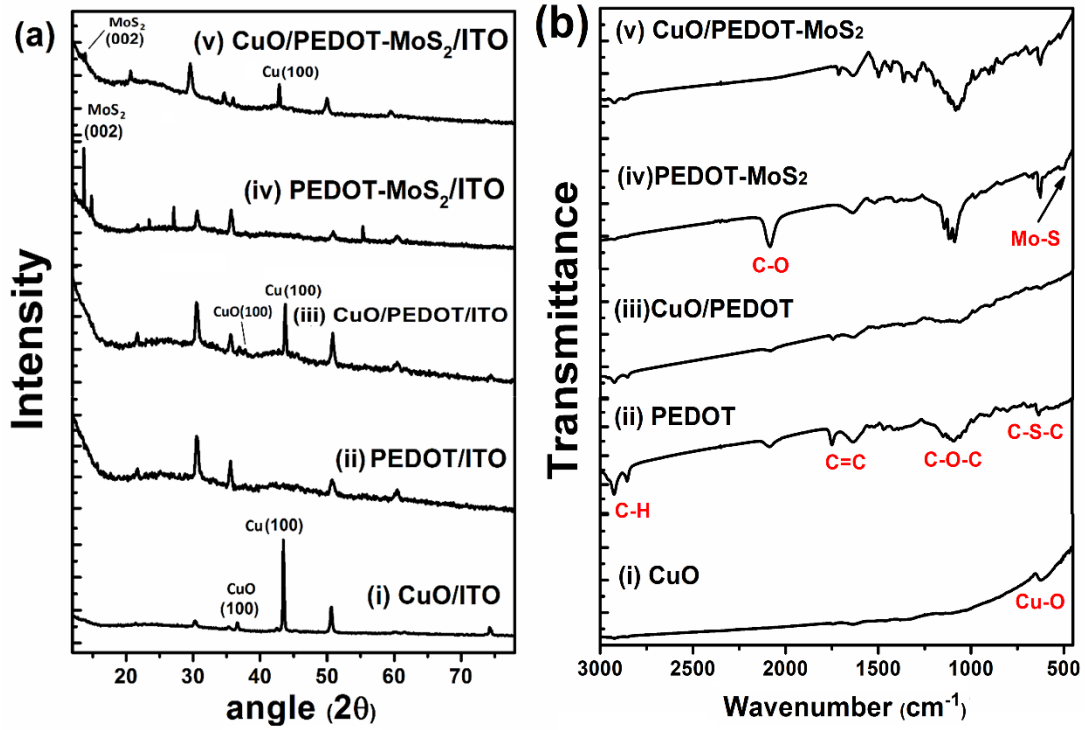

Figure 4.2: (a) XRD patterns, and (b) FT-IR spectra of as-synthesized CuO, PEDOT, CuO/PEDOT, PEDOT-MoS_2 and CuO/ PEDOT-MoS_2 systems

The samples for FT-IR were collected by peeling off the deposited films from the ITO coated glass as described in section 2.3.2. Figure 4.2(b), depicts a series of FT-IR spectra of all the five samples: CuO, PEDOT, CuO/PEDOT, PEDOT-MoS_2 and CuO/PEDOT-MoS_2 denoted by graph (*i*)-(*v*), in sequence. The band at 622 cm^{-1} and shown in curve-(*i*) essentially signifies the Cu-O bond vibration [189]. As shown in curve-*(ii)*, the FT-IR spectrum of PEDOT offers several distinct peaks at their specific position as discussed in section 3.3.1. The CuO deposited PEDOT film exhibited less prominent absorption bands as compared to the PEDOT specimen (curve- (*iii*)). This indicates that electrodeposition of CuO over PEDOT has modified the spectral features of the polymer

matrix. The peak appearing at ~510 cm^{-1} in trace-(*iv*) confirms the presence of Mo-S vibrational band in the PEDOT-MoS_2 composite [190]. Interestingly, the intensity of PEDOT peaks would increase after incorporation of exfoliated MoS_2 in the matrix followed by the appearance of sharp C-O vibrational band at, ~2080 cm^{-1} which got suppressed in PEDOT and CuO/PEDOT systems. This was believed to be due to the relaxing of the PEDOT vibrational modes after incorporation of the layered MoS_2 in the polymer. After deposition of Cu NPs, the PEDOT-MoS_2 peaks became less intense, and the C-O peak disappeared completely, as can be seen from the spectrum-(*v*). We anticipate the electrodeposited, inorganic metal NPs to suppress the intermolecular relaxation of the polymer-TMDC composite featuring a completely different spectrum.

4.3.2. Morphological features and elemental analyses

Similar protocol has been followed as mentioned in section 2.3.1 to prepare the samples for morphological assessment. In Figure 4.3 (a-e), each set essentially characterize two FE-SEM micrographs captured at lower and higher magnifications along with the EDX spectrum shown in the right. The inner shell electronic absorption spectra of the EDX response confirm the elemental constituents present in our samples. The FESEM micrograph shows a fairly uniform distribution of the electrodeposited CuO NPs with partial agglomeration over the smooth ITO substrate (Figure 4.3(a)). The EDX response shows the *K*-shell absorption spectra of Cu and O that confirms the formation of CuO in the film. The presence of a lower atomic % of O with respect to Cu would indicate that the outer layer of the nanoparticles can experience effective oxidation while the inner atoms remained unoxidized. Also, it is possible that the creation of oxygen vacancies/point defects in the synthesized NPs may lead to higher atomic % of Cu. The homogeneous distribution of electropolymerised PEDOT over the electrode is shown in Figure 4.3(b) and from the magnified image one can clearly see the PEDOT grains covering the whole substrate, thereby resulting in an increased surface roughness. These conductive PEDOT grains not only incease the surface roughness of the solid film but also provide a larger surface area for the electrodeposition of CuO NPs. The surface coverage of the PEDOT film by metal oxide NPs where the formation of polymer clusters can be seen over the surface due to the deposition of Cu NPs is shown in Figure 4.3(c). In case of CuO/PEDOT, these electrodeposited metal NPs act as a binder to wrap the polymer grains together to form larger clusters.

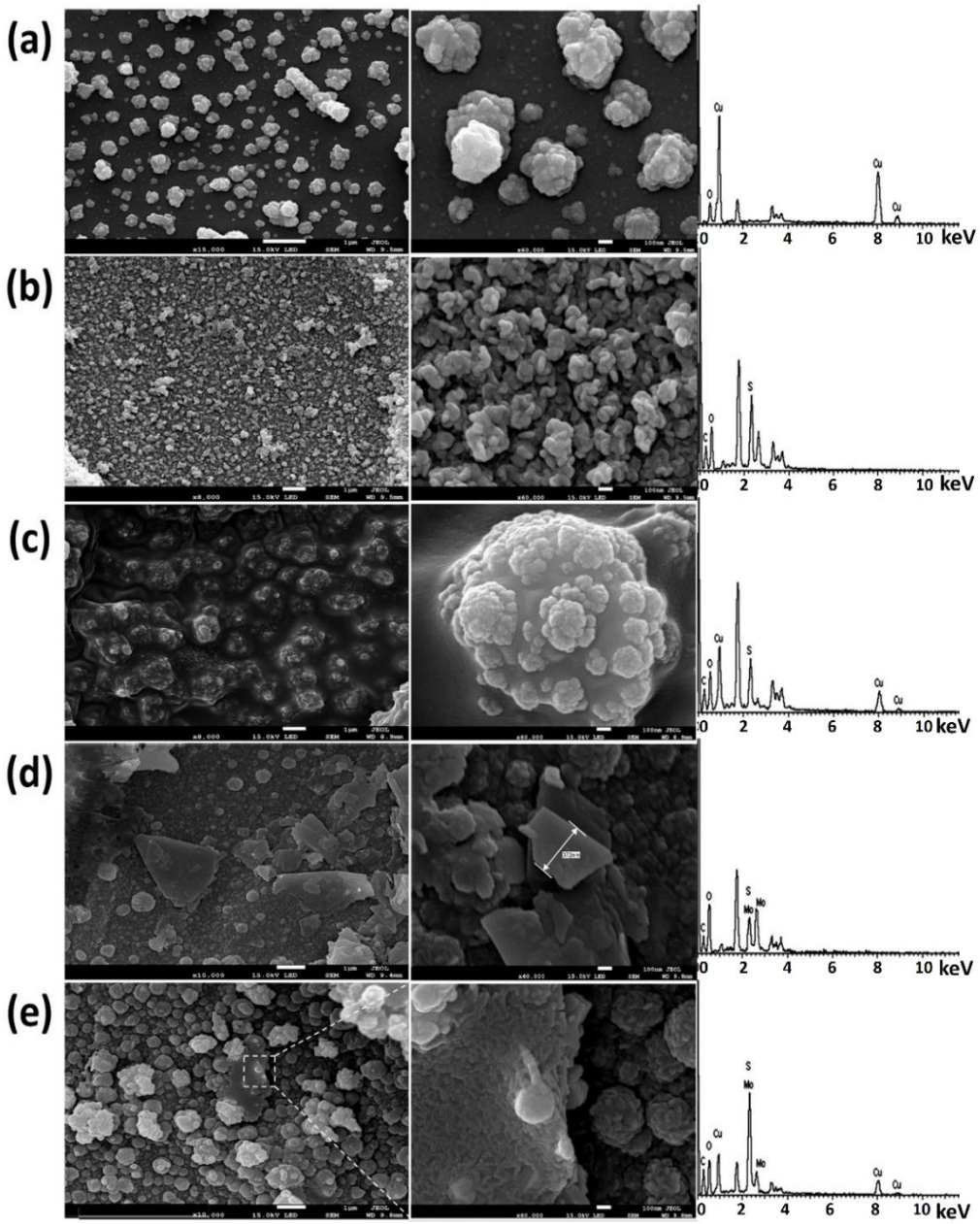

Figure 4.3: FESEM micrograph of (a) CuO, (b) PEDOT, (d) CuO/PEDOT, (d) PEDOT-MoS_2, and (e) CuO/PEDOT-MoS_2 along with the EDX spectra shown on the right-hand side

The deposition of the metal NPs over the conductive surface of large grain cluster of the polymer is also shown. Here, rather than agglometarion of Cu NPs as observed in the case of ITO substrate, they seem uniformly deposited over the PEDOT. The presence of all the elemental constituents of PEDOT and CuO/PEDOT can be traced in the EDX spectra, as shown in Figure 4.3(b) and (c). The FE-SEM image of MoS_2 incorpoated PEDOT film can be found in Figure 4.3(d). Here, we expect electropolymerization of EDOT in presence

of exfoliated MoS_2 sheets, leading to the formation of the polymer film by entrapping the MoS_2 sheets of different areal dimension in and over the PEDOT matrix. Also, from the *L*-shell absorption spectra of Mo in the inserted EDX pattern of Figure 4.3(d) confirms the incorporation of MoS_2 in the PEDOT matrix. The rough surfaces of the PEDOT-MoS_2 films confirm the effective deposition of metal NPs over the polymer-TMDC composite system. Herein, we can clearly view the MoS_2 flakes dispersed in the polymer along with Cu NPs over the surface of the composite film. The appearance of C, O, Cu, S and Mo inner shell absorption spectra in the EDX of Figure 4.3(e) substantiates presence of relevant elements in the CuO/PEDOT-MoS_2 composite system.

4.3.3. Cyclic voltammetry and impedance spectroscopy studies

All electrochemical measurement in this work have been accomplished by using a three-electrode setup as described in section 2.3.5. CV response of the fabricated electrodes was acquired a scan rate of 20 mV/s across the potential window of -0.2 to +0.7 V. As can be noticed, with the use of PEDOT polymer the current response of the CV- cycle increases substantially as compared to the mere electrodeposited CuO NPs (Figure 4.4(a)). To be mentioned, the conducting polymer matrix not only provides a higher surface area for the electrodeposition of CuO but also enhances the electron transfer mechanism by hopping of carriers in addition to doping/de-doping of electrolytic ions in the polymer matrix at varying potential [191]. Moreover, incorporation of MoS_2 nanoflakes in the PEDOT host matrix has further augmented the current response of CV as can be seen in Figure 4.4(a). MoS_2 being a conductive 2D layered structure is believed to enhance the electron transfer synergistically by way of shortening the diffusion path length for the ion transport in the composite CuO/PEDOT-MoS_2.

Impedance spectra for all the three systems under study were acquired in the frequency range of 0.1 Hz- 1 MHz at an applied DC bias voltage of 0 V w.r.t. the reference, as shown in Figure 4.4(b). The long tail observed at the lower frequency region for CuO electrode indicates high Warburg impedance (W_z) due to carrier diffusion. The magnified portion of the EIS plot in the high frequency region and the fitted spectra with corresponding equivalent circuit is inserted in Figure 4.4(b). In fact, all the three systems follow the same Randle equivalent circuit, shown in the Figure 4.4(b). In the equivalent circuit, all the parameters retain their conventional interpretations as discussed in section 2.3.6. The R_{ct} value drops from 38.93 Ω to as low as 7.31 Ω after incorporation of MoS_2 in the PEDOT matrix as compared to CuO only electrode, thereby indicating significant

interfacial charge transfer in the whole CuO/PEDOT-MoS_2 system. The C_{dl} value drops upon inclusion of MoS_2 in the PEDOT, resulting an efficient faradic charge transfer that would occur at the electrode-electrolyte interface. Additionally, C_3 is the augmented capacitance that may arise due to the development of interfaces/interlayers in between CuO-PEDOT and MoS_2-PEDOT polymer composites. Moreover, the concentration gradient that appears due to the movement of counter ions towards the W.E. hinders the smooth mass transport in the electrolyte solution. This results in diffusion phenomena as well as Warburg impedance in the electrolyte-electrolyte system.

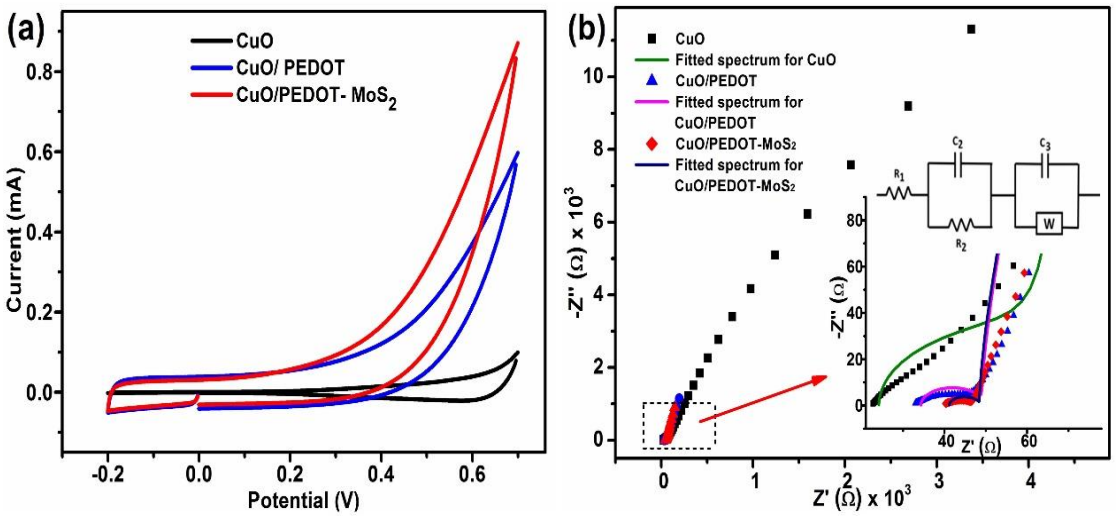

Figure 4.4: (a) Cyclic voltammetry (CV) response, and (b) electrochemical impedance spectroscopy (EIS) plots of CuO only, CuO/PEDOT and CuO/PEDOT-MoS_2 electrodes. A magnified view of the segment in -Z" vs. Z' plot as well as equivalent RC circuit are also shown as inset in (b)

Table 4.1: EIS derived physical parameters obtained after proper fitting.

Electrodes	R_1 (Ω)	R_2 (Ω)	$C_2\times10^{-6}$ (F)	$C_3\times10^{-6}$ (F)	$W\times10^{-6}$ ($S*s^{1/2}$)
CuO	24.16	38.93	20.23	61.44	54.95
CuO/PEDOT	34.31	14.66	25.08	1078	369.80
CuO/PEDOT-MoS_2	41.14	7.31	18.98	1379	437.16

4.3.4. Glucose oxidizing activity of the sensor electrodes

Glucose oxidation with the synthesized electrodes could be visualized from the CV responses in presence and absence of glucose present in the solution. The CV was taken under the potential window of -0.2 to +0.7 V at a scan rate of 20 mV/s in 0.1 M NaOH solution as shown in Figure 4.5(a-c). In absence of glucose, there is no peak/hump in the CV responses. But current increases in the oxidation region upon addition of glucose and if one varies the glucose concentration from 0.1 mM to 0.5 mM, then oxidation current also increases monotonically as per the concentration of added glucose in the solution. In the figures, one can see that upon addition of glucose, the oxidation current would increase around +0.3 V followed by the appearance of an oxidation hump around +0.4 V and this hike in the current remains constant up to +0.6 V. Upon comparison of the three CV responses, a synergistically enhancement in current could be obtained in favour of CuO/PEDOT-MoS_2. Without doubt, it offers a potentially more efficient electrode candidate for non-enzymatic sensing of glucose.

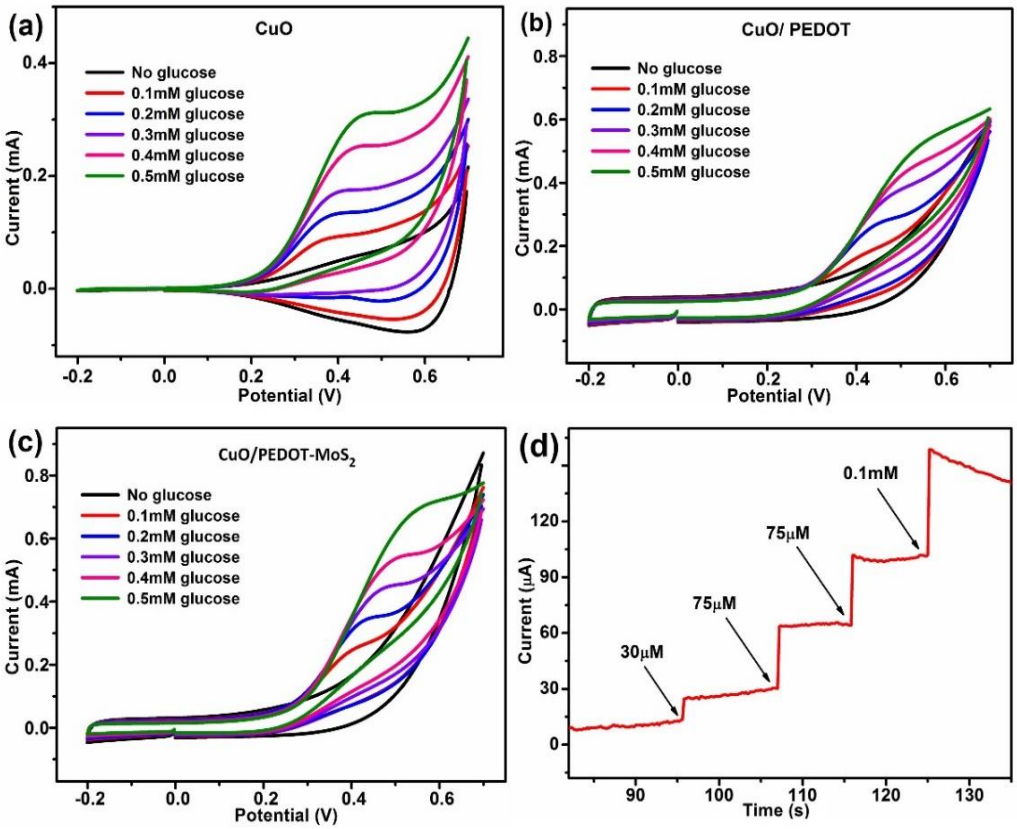

Figure 4.5: CV responses of (a) CuO/ITO, (b) CuO/PEDOT and (c) CuO/PEDOT-MoS_2 at different concentration of glucose varying from 0.1 to 0.5 mM, (d) chronoamperometric response of CuO/PEDOT-MoS_2 sensor over different glucose concentration at +0.6 V dc potential

As the glucose concentration was varied unevenly, the CV responses of Figure 4.5(a-c) showed an enhanced, stabilized current over +0.6 V for the test electrodes in 0.1 M NaOH solution. This is the reason why the said voltage was considered w.r.t. reference as a fixed dc bias potential in the amperometric (*i-t*) feature, presented in Figure 4.5(d). Different concentration of glucose was added to observe the activity of CuO/PEDOT-MoS_2 sensor in 0.1M NaOH solution at a dc bias potential of +0.6 V and a significant enhancement in amperometric current could be obtained in the *i-t* response after every addition of glucose in the solution.

4.3.5. Estimation of electrochemical parameters

To quantify the electroactivity of the electrode materials, estimation of several critical electrochemical parameters is necessary. For instance, diffusion coefficient of the redox species towards the electrode, electroactive area of the electrode, reaction rate constant of the redox process, etc. In this section, our primary motive was to calculate the electroactive area of the specimen electrodes for oxidation of glucose in 0.1M NaOH solution by using Randle-Sevcik equation [192]. To do so, the diffusion coefficient (*D*) of glucose towards the surface of the synthesized electrode systems need to be determined. The estimation of *D* can be ascertained through the Cottrell equation which gives a relation between the amperometric current *(I_t) vs.* time (*t*) as given below [193]:

$$I_t = nFD^{1/2}C\pi^{-1/2}A_o t^{-1/2} \ , \qquad (4.1)$$

here, C' (= 0.2 mM) is concentration of glucose, A_o (= 0.5 cm^2) is geometrical area of the electrode and all other parameters bear the similar meaning as outlined in Eq. 3.1 and 3.2 of Chapter 3. For a single electron transfer process (*n*=1), the slope (ς) of the obtained I_t *vs.* $t^{-1/2}$ plot can be expressed as,

$$\varsigma = nFD^{1/2}C'\pi^{-1/2}A_o$$

$$\text{or,} \qquad D = \frac{\pi\varsigma^2}{n^2F^2A_oC'^2} \qquad (4.2)$$

The single step chronoamperometric response of the synthesized electrodes were taken for 30 s in presence and absence of glucose in the solution, as depicted in Figure 4.6(a). After addition of 0.2 mM glucose the amperometric current response increases (represented by scattered red lines), as can be seen in Figure 4.6(a). The I_t vs. $t^{-1/2}$ could be plotted from the dynamic amperometric response obtained after the addition of 0.2 mM glucose where the slope of the linear-fit is proportional to the diffusion coefficient (*D*), as mentioned in equation 4.2 (Figure 4.6(b)).

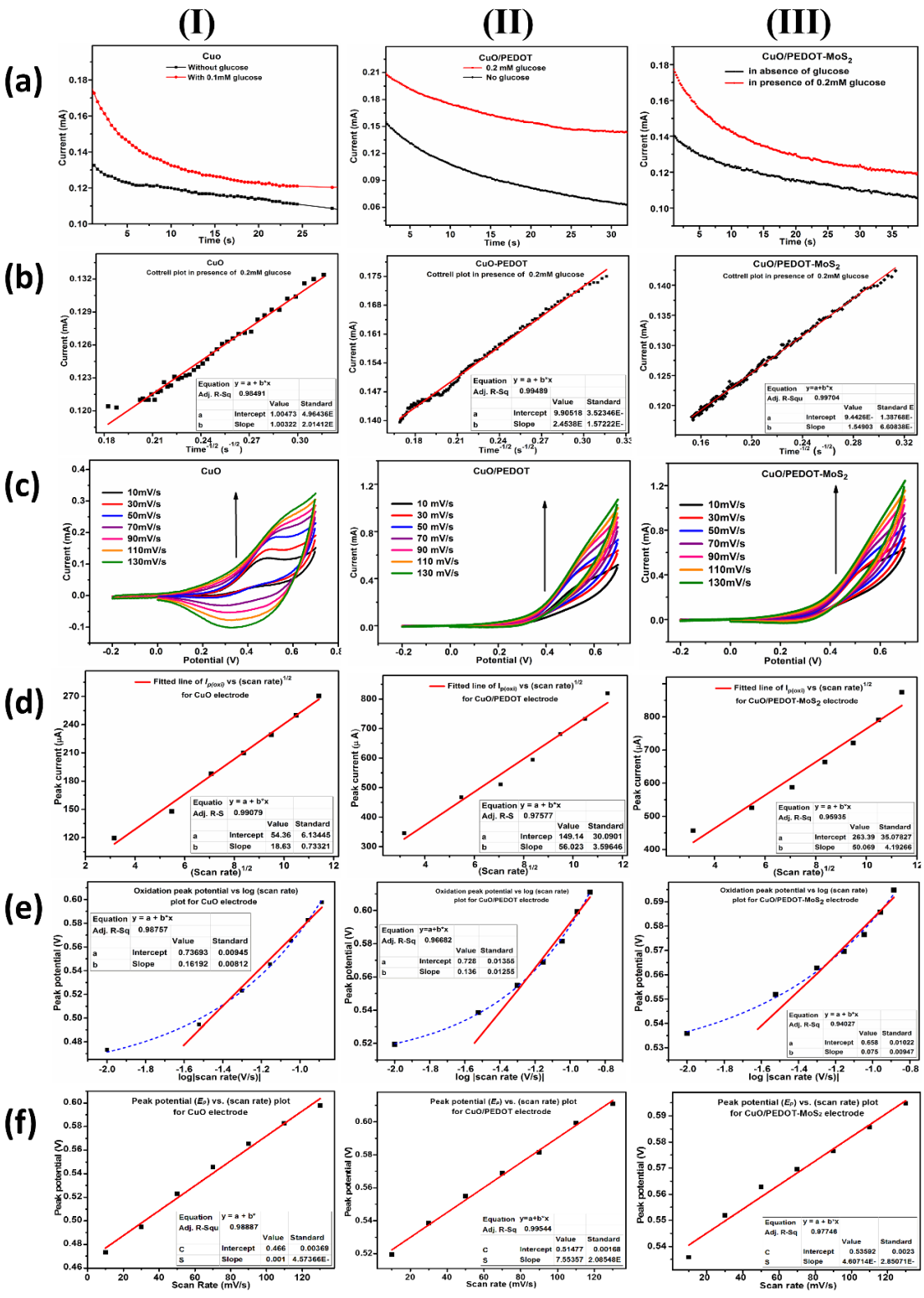

Figure 4.6: (a) Amperometric (*i-t*) response in presence and absence of 0.2 mM glucose, (b) Cottrell plot (*i vs* $t^{-1/2}$), (c) current vs. voltage response with scan rate variation in cyclic voltammetry (CV), (d) Randle- Sevcik (i_p *vs* $v^{1/2}$) plot, (e) E_p vs *log | (scan rate) |* plot and (f) Peak potential (E_p) vs (scan rate) plot; for (I) CuO only, (II) CuO/PEDOT, and (III) CuO/PEDOT-MoS_2 electrode systems.

In the present case, the calculated values of diffusion coefficients are 1.7×10^{-4} cm^2/s, 9.1×10^{-4} cm^2/s, 4.3×10^{-4} cm^2/s for the CuO only, CuO/PEDOT and CuO/PEDOT-MoS_2; respectively. The CV responses of these electrode systems were acquired by varying the scan rates, from 10 mV/s to 130 mV/s and considering 0.1 M NaOH as the electrolyte and 0.2 mM glucose as redox entity (Figure 4.6(c)). Here, the current in the anodic region increases upon increasing the scan rate due to the irreversible conversion of glucose into gluconic acid through oxidation process [194]. The appearance of the cathodic peak is due to the reduction of *Cu (III)* to *Cu (II)* itself, as glucose oxidation is an irreversible charge transfer process. In Figure 4.6(d), the good linear fitting of anodic peak current (i_p) with square root of the scan rate ($\sqrt{\upsilon}$) indicates the occurrence of diffusion-controlled process in the system under study [195]. In such irreversible redox process, the relation between i_p and υ is represented in accordance with the Randle-Sevcik proposition [**196-198**], as follows: $i_p = 0.4463 \times nFAC(\frac{nF\upsilon D}{RT})^{\frac{1}{2}}$ and at room temperature (T=300 K), we would obtain,

$$i_p = 2.69 \times 10^5 \times n^{3/2} A D^{1/2} C \upsilon^{1/2} \qquad (4.3)$$

Also, we can write electroactive area, $A = \frac{\varsigma}{2.69\times10^5\times n^{3/2} C D^{1/2}}$. From the slope of the i_p vs. $v^{1/2}$ plot shown of Figure 4.6(d), the electroactive area for the CuO, CuO/PEDOT and CuO/PEDOT-MoS_2 are estimated as, ~ 0.81 cm^2, 1.10 cm^2, and 1.47 cm^2; respectively. There is a significant impact on increasing the electroactive area of the transducer after incorporation of MoS_2 in PEDOT, as can be found in Table 4.2. Lastly, Laviron's equations for the irreversible process are employed to study the electron transfer kinetics of the electrode for oxidation of glucose as follows [199]:

$$E_p = E_o' - \frac{2.3RT}{\alpha nF} log \frac{RTk_s}{\alpha nF} + \frac{2.3RT}{\alpha nF} log\upsilon \qquad (4.4)$$

In the above equation, E_p is the peak redox potential, E_o' is formal standard potential, α is transfer coefficient and k_s is heterogeneous rate constant. By solving the equation (4.4), we can easily determine the values of α and k_s. For this purpose, the peak potential (E_p) *vs. log (υ)* and the $E_p = f(log\ \upsilon)$ plot yielded a straight line with slope equivalent to $\frac{2.3RT}{\alpha nF}$, as depicted in Figure 4.6(e). For the oxidation of glucose by CuO/PEDOT-MoS_2 electrode, the value of the transfer coefficient (α) is also calculated. The values of formal standard potential (E_o') are estimated from the *y*-intercept of the linearly fitted line of the peak potential (E_p) vs. scan rate (v) plot [200] (supplied in Figure 4.6(f)). Now, putting the value

of α and solving equation 4.4, the heterogeneous electron transfer rate constant (k_s) for CuO, CuO/PEDOT and CuO/PEDOT-MoS_2 electrode systems can be determined. Accordingly, the respective values are, 0.30 s^{-1}, 0.46 s^{-1} and 0.76 s^{-1}. This illustrates the synergic enhancement in the electron transfer kinetics as we modify the CuO deposited transducer with layered MoS_2 and conducting polymer system.

Table 4.2: Estimated electrochemical parameter of the three system electrodes.

Electrodes	D (cm^2/s) $\times 10^{-4}$	A (cm^2)	α	k_s (s^{-1})
CuO	1.7	0.811	0.355	0.30
CuO/PEDOT	9.0	1.10	0.434	0.46
CuO/PEDOT-MoS_2	4.1	1.47	0.787	0.76

4.3.6. Amperometric detection of glucose and selectivity test

Sensing of glucose by CuO, CuO/PEDOT and CuO/PEDOT-MoS_2 electrodes are performed by chronoamperometric technique at a fixed dc potential of +0.6 V w.r.t. the Ag/AgCl in 0.1M NaOH solution. Typical *i-t* plots of the three electrodes with successive addition of glucose at different concentrations are shown in Figure 4.7(a). The increase in current value monitored in the amperometric response after each addition of glucose in the solution indicating that glucose oxidation has taken place over our sensor electrode at a dc bias potential of +0.6 V. It was seen that the *i-t* response of CuO NP only electrode requires more time to stabilize after the injection of glucose and the current response tending to saturate at 0.75 mM. While in case of CuO/PEDOT system, the response time for glucose detection declines and one gets a relatively lower current response with the corresponding addition of glucose. In contrast, CuO/PEDOT-MoS_2 electrode exhibits a notable current change at a lower concentration of glucose. Moreover, here, we observe a higher magnitude of current as compared to the other two electrodes upon successive additions of glucose. Thus, the CuO deposited PEDOT-MoS_2 electrode seems to be a better electrode material for glucose sensing. The selectivity of the prepared sensor towards glucose has been confirmed by testing its interaction with other coexisting interfering molecules like ascorbic acid (AA), uric acid (UA) and hydrogen peroxide (H_2O_2) during the acquisition of amperometric *i-t* characteristics, as can be found in Figure 4.7(b). Although the glucose level in blood is normally ten times higher than these species, but interactions of these interferents with our prepared sensor electrode needed a close inspection for a reliable glucose monitoring. Accordingly, H_2O_2, ascorbic acid and uric acid were added in the

solution (each having concentration of 0.1 mM) to check their interaction with CuO/PEDOT-MoS_2 through the *i-t* feature taken at +0.6 V.

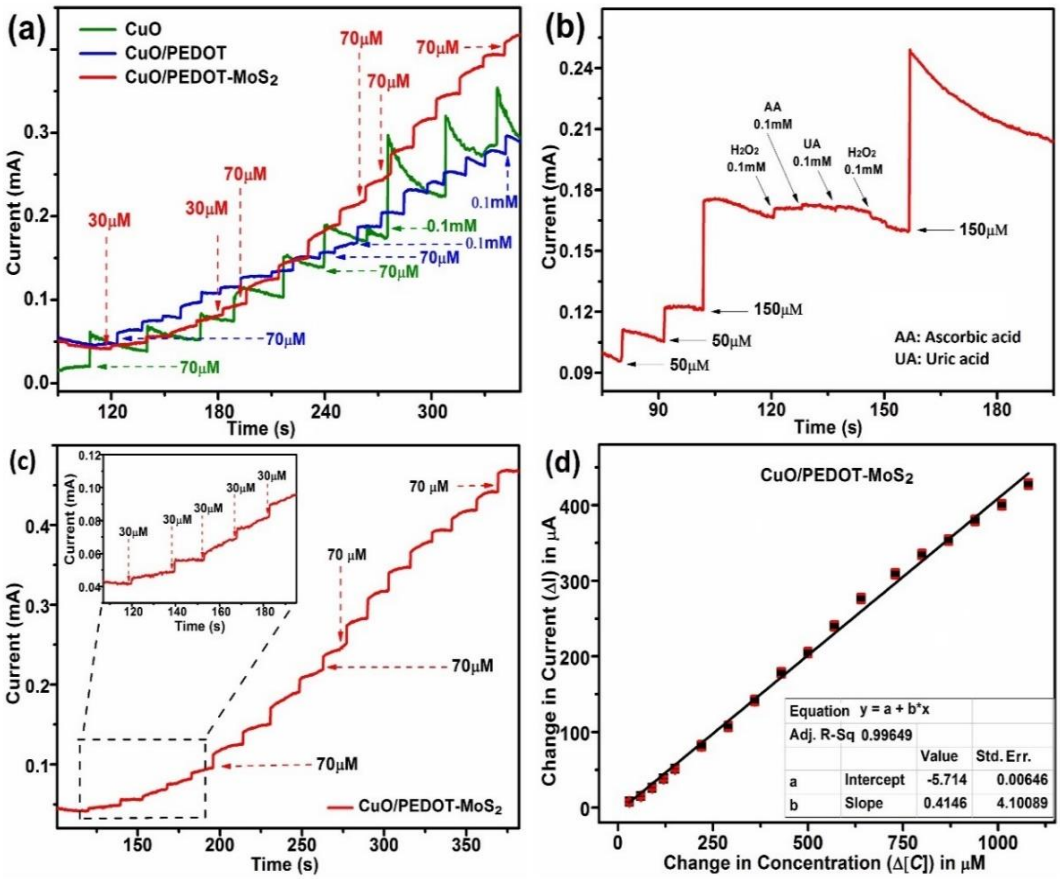

Figure 4.7: (a) Merged amperometric (*i-t*) response of CuO, CuO/PEDOT and CuO/PEDOT-MoS_2 electrode, (b) selectivity test of CuO/PEDOT-MoS_2, (c) amperometric response of the CuO/PEDOT-MoS_2 with inset magnified portion, (d) change in (*i-t*) current (ΔI) vs. change in concentration ($\Delta[C]$) plot

To be mentioned, the plot shows an augmented current response on addition of varying concentration of glucose in first three subsequent steps. However, addition of H_2O_2, AA, and UA of 0.1 mM each in the solution did not show any remarkable change in *i~t* response towards these aforesaid analytes. It is worth mentioning here that, an additional 150 µM of glucose in the solution could result in an enhancement in the amperometric current. Therefore, MoS_2 infiltrated PEDOT based sensor displays a substantially high redox activity and consequently, high selectivity for glucose. The *i-t* response of CuO/PEDOT-MoS_2 plot along with the magnified portion of the curve featuring response at a lower concentration of glucose addition can be found from Figure 4.7(c). First, the chronoamperometry experiment was ran and the response was allowed to attain a stable

baseline after which 30 µM glucose is added. The concentration of glucose in the solution would increase upon subsequent additions, featuring a proportional rise in the measured amperometric current. The change in current (ΔI) vs. corresponding concentration of added glucose (*[C]*) can be found in Figure 4.7(d). Here, the error bars were assigned w.r.t. the standard deviation of current change *(*ΔI), corresponding to all glucose additions having similar concentration (*e.g.*, a standard deviation of 2.56 µA is obtained for the first six additions of glucose having 30 µM concentrations each). The plot shows a good linearity in the concentration range of 30 µM to 1.06 mM and with a regression equation, $y = 0.414x - 5.71$; where, y is current shift in the amperometric response and x is corresponding concentration of glucose. From the linear plot of Figure 4.7(d), the *LOD* of CuO/PEDOT-MoS_2 based sensor was estimated to be 0.0467 µM and with a sensitivity value of 829 µA. $mM^{-1}cm^{-2}$.

4.3.7 Stability, repeatability and reproducibility test of the sensor electrode

(a) Stability test

The electrochemical stability of our CuO/PEDOT-MoS_2 composite based sensor electrode was examined by running the cyclic voltammetry (CV) for 25 cycles at a scan rate of 20 mV/s under the potential window of -0.2 V to +0.7 V in 0.1 M NaOH solution. In Figure 4.8, we see a normal decrease in current response after each CV cycles. A little diminution in the CV current was observed after 2nd cycle; whereas, the response almost remains uniform between 3rd to 20th cycles with an insignificant current change after subsequent run of CV. Although the prepared electrode offers good electrochemical activity upto 25th cycles, but the lowering of the CV area indicates a degradation of the metal oxide-polymer composite over higher number of CV runs.

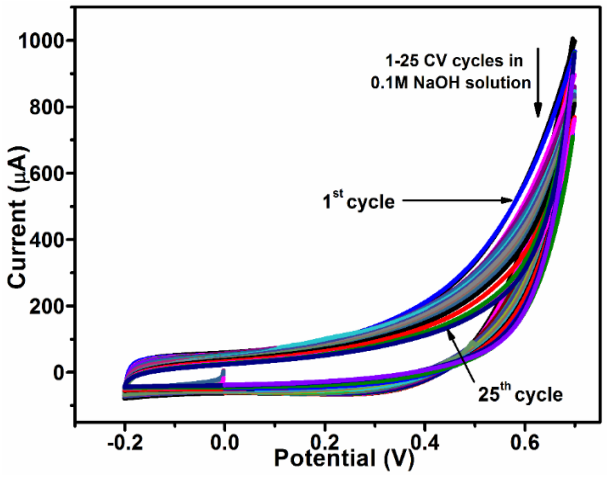

Figure 4.8: Stability test for CuO/PEDOT-MoS_2 sensor electrode

(b) Repeatability test

The chronoamperometric responses (3 sets) of the composite sensor electrode towards sensing glucose in 0.1 M NaOH solution at an applied dc bias potential of +0.6 V w.r.t. the reference can be found from Figure 4.9. All the three curves followed similar trends with equivalent proportion of current change corresponding to each concentration of added glucose. In the 1st response, 30 μM of glucose was added for 8 times, and in other two cases, 30 μM of glucose was added upto 6 times. Here, all the three responses exhibited almost equivalent current shift (from the initial position) over addition of a sum of ~1 mM glucose in the solution which affirms repeatability of the as prepared sensor. The sensing parameters like *LOD*, sensitivity, etc. are calculated for all the three responses, shown in Table 4.3. Also, the values of *LOD* and sensitivity obtained from all the 3 repeated experiments were plotted and compared in the histogram, as depicted in Figure 4.9(d) and (e), where the error bars are assigned w.r.t. the standard deviation of the values obtained from all the repeated experiments. The overlapped error bars of Figure 4.9(d) and (e) would signify that the *LOD* and sensitivity values obtained (from all the sensing experiments) are quite indifferent from each other.

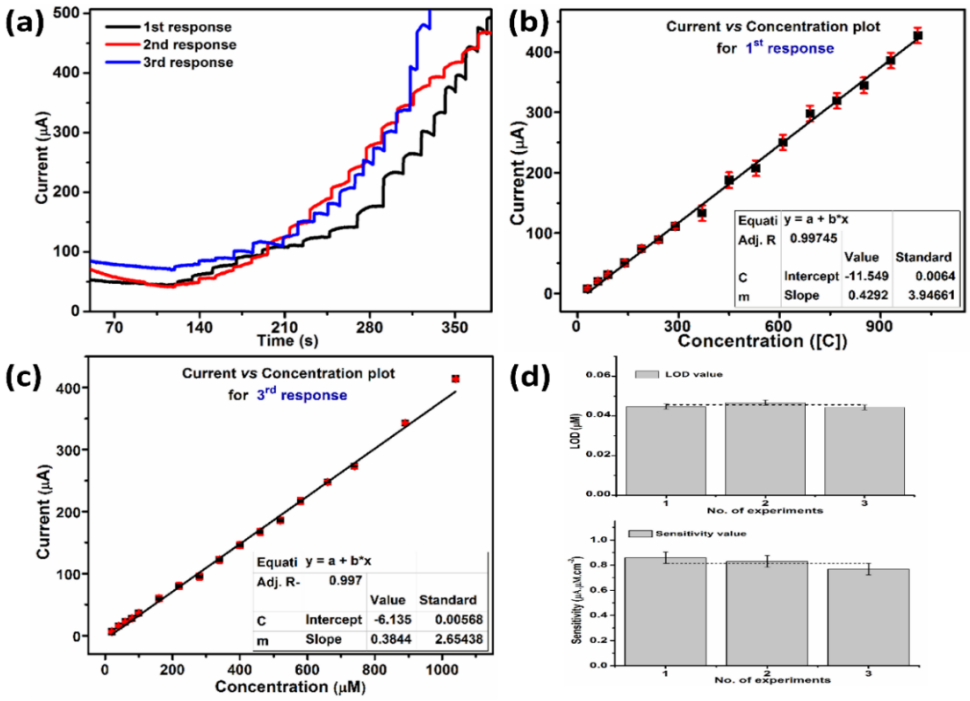

Figure 4.9: (a) Repeatability tests for the CuO/PEDOT-MoS_2 sensor electrode, change in current (ΔI) vs. concentration ($\Delta[C]$) plot for chronoamperometric, (b) response-1 and (b) response-3, and histograms of the (d) *LOD*, and (e) sensitivity values

Table 4.3: *LOD* and sensitivity values estimated from the three repeated experiments.

Sl. no. of expt.	*LOD* (µM)	Sensitivity (µA. µM.cm^{-2})
1.	0.0447	0.858
2.	0.0467	0.829
3.	0.0443	0.768

(c) Reproducibility test

The reproducibility test of the fabricated sensor was monitored by taking the CV response of CuO/PEDOT-MoS_2 electrode on 1st, 2nd, 3rd, 5th, 7th,10th and 14th day, in presence of 0.2 mM glucose. In CV cycles, the oxidation current obtained at +0.6 V (which was considered as glucose oxidizing potential in the system) is compared accordingly for the multiple use of the same electrode towards oxidizing glucose. Here, Figure 4.10(a) depicts the CV response of the composite system in absence and presence of 0.2 mM glucose in 0.1 M NaOH solution, where a broad hump in the oxidation region can be seen due to the redox process of glucose oxidation. Afterwards, the CV response of the same electrode (in presence of 0.2 mM glucose) was monitored on 2nd, 3rd, 5th, 7th, 10th and 14th day after taking the first response, as shown in Figure 4.10(b). The oxidation current corresponding to +0.6 V is plotted in the histogram plot w.r.t. no. of days as shown in Figure 4.10(c), where the error bars were assigned with regard to standard deviation of the current response. It has been found that the % recovery of the sensing performance is exceptionally good upto five days and it gets deteriorated upto 84.0% on 14th day of testing (Table 4.4).

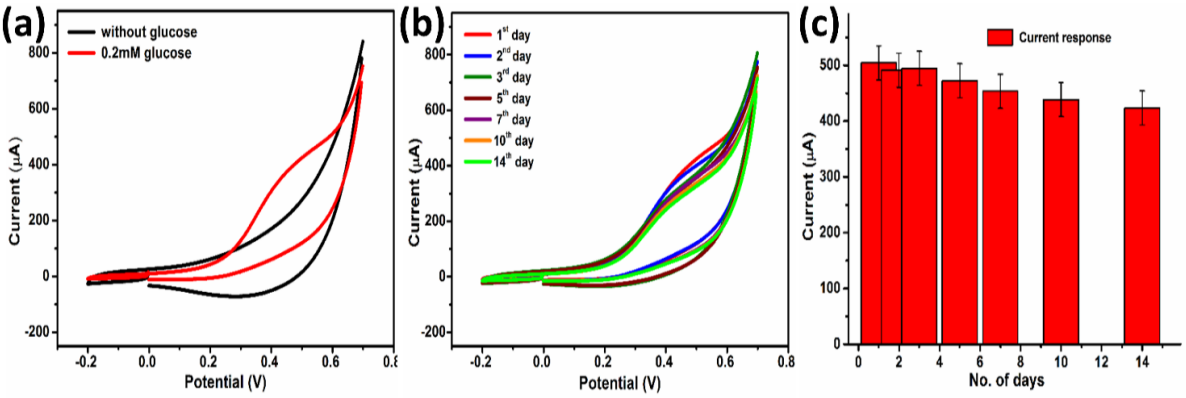

Figure 4.10: CV responses of CuO/PEDOT-MoS_2 (a) in presence and absence of glucose, (b) on different days. (c) Histogram plot of oxidation current response of the sensor on different days

Table 4.4: % recovery of the current response of the sensor after multiple experiments.

Days	Current response (μA)	% Recovery
1st day	504.09	---
2nd day	490.87	97.4
3rd day	494.61	98.2
5th day	472.18	93.7
7th day	453.44	90.0
10th day	438.55	87.0
14th day	423.60	84.0

4.3.8. Real sample test

The validity of the prepared glucose sensor was examined by determining the glucose concentration in a commercially available oral rehydration solutions (ORS), which contains 75% glucose along with other minerals like Na, K, Cl, etc. At first, aqueous ORS samples (prolyte^{TM}, Cipla) were prepared having different glucose concentration. The glucose level in the prepared ORS samples were then cross-checked by using our sensor module. Three sets of chronoamperometric response were taken in 0.1M NaOH solution at an applied bias potential of +0.6 V w.r.t. the reference as shown in the Figure 4.11 (a-c). During each experiment, ORS samples with varying glucose concentration were added in the solution (Figure. 4.11) and the corresponding change in *i-t* response was monitored. The concentration of glucose in the added ORS samples were determined by using the as proposed calibration equation (see section 4.3.6): $x = \frac{y+5.71}{0.414}$; where, *y* is the current shift in the amperometric response and *x* is corresponding concentration of glucose. The estimated and the real values of glucose concentrations in the ORS samples are compared in the Table 4.5, and the corresponding relative % error were found to lie in between ~ ± (1-2) %. The standard error (S.E.) of experiment (b) and (c) was also determined to be 1.54 and 1.48; respectively. The lower value of S.E. suggests high reliability of our prepared sensor towards determining glucose level in real samples.

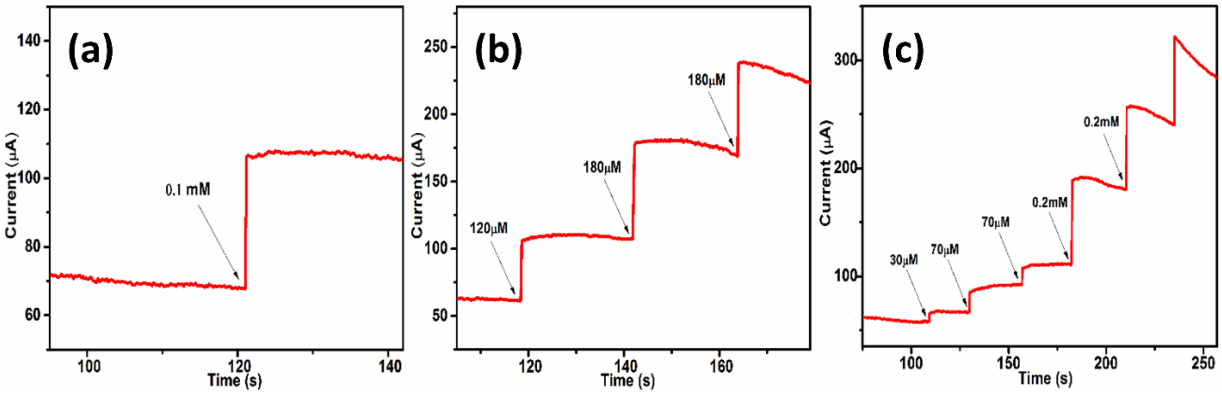

Figure 4.11: Chronoamperometry response of CuO/PEDOT-MoS_2 sensor electrode for determining glucose concentration in commercially available ORS solution.

Table 4.5: Comparison of real and estimated glucose concentration in the ORS samples.

Experiment	Real concentration of glucose in the ORS sample	Concentration obtained from calibration curve	Relative % Error	Standard error
(a)	100 µM	102.55	2.55	--
(b)	120µM	121.73	1.73	1.54
	180µM	183.18	1.59	
	180µM	177.46	-1.26	
(c)	30µM	30.62	2.06	1.48
	70µM	70.33	0.47	
	70µM	69.08	-1.31	
	0.2mM	203.27	1.63	
	0.2mM	201.95	0.975	

4.4. Conclusions

Structural, morphological and elemental studies were carried out for electrochemically deposited CuO, CuO/PEDOT and CuO/PEDOT-MoS_2 films and then employed for sensing AR-grade glucose and commercially available ORS. Among these electrodes, the latter ensured a better redox activity as well as better charge transfer efficiency. Different electrochemical parameters *viz*. diffusion coefficient (D), electroactive area (A) and heterogeneous rate constant (k_s) for the synthesized electrodes towards oxidation of glucose in 0.1 M NaOH solution were estimated and compared. Direct sensing of glucose was performed by chronoamperometric technique for all the electrode-types and a much better

response could be obtained for the PEDOT-MoS_2 electrode. The fabricated sensor endorsed a fairly good selectivity towards glucose in a wide linear range of 30 μM-1.06 mM. The *LOD* and sensitivity of the sensor under study were estimated to be 0.046 μM and 829 μA $mM^{-1}cm^{-2}$; respectively. As compared to many other electrode materials, the CPs are relatively less toxic and subject to degradation after use. Also, incorporation of CPs with the electroactive metal oxide nanoparticles certainly calls for a new test-bed of an organic-inorganic hybrid system for better non-enzymatic detection of the target redox analyte. The designed sensor electrode is expected to detect precisely small glucose level with excellent selectively in biological solutions and commercial food products.

In the electrochemically synthesized CuO/PEDOT-MoS_2 based sensor probe, the polymer matrix offers high surface area, enhances conductivity and allows better incorporation of MoS_2 layered nanostructures in the composite film. But other synthesis procedure can deal with all-inorganic material-based composite electrocatalyst without consideration of a polymer matrix. Moreover, the morphology of the host electrocatalyst plays a critical role in the catalytic activity of a non-enzymatic sensor. Since electrochemical deposition technique has very limited control over the morphology of the deposited nanoparticles, alternative chemical techniques can be opted for. In addition, employing the same sensor probe for detection of multiple analytes can be attractive and is an important advancement in the field of electrochemical sensing. Subsequent chapter will discuss about the selection of a new electrocatalyst system with modified morphology which can full fill the demand of multiple use of analytes employing the same electrode.